Journal of Advanced Joining Processes 9 (2024) 100177

Contents lists available at ScienceDirect

Journal of Advanced Joining Processes

journal homepage: www.sciencedirect.com/journal/journal-of-advanced-joining-processes

Thermographic procedure for the assessment of Resistance Projection Welds (RPW): Investigating parameters and mechanical performances

G. Dell'Avvocato *, D. Palumbo

Department of Mechanics, Mathematics and Management, Polytechnic University of Bari, Via Orabona 4, Bari 70125, Italy

ARTICLE INFO

Keywords:
Flash thermography
Mechanical properties
Non-destructive testing (NDT)
Resistance Projection Welding (RPW)
Pulsed phase thermography
Welding assessment

ABSTRACT

This study presents a non-destructive testing (NDT) thermographic procedure for assessing the quality and mechanical strength of Resistance Projection Welded (RPW) joints with rectangular embossments. We analysed twelve RPW joints by systematically varying process parameters based on a factorial design. These joints underwent flash thermography followed by mechanical tests to evaluate the maximum breaking force (F_{max}). Significant statistical correlations between process parameters (time and force) and F_{max} were established. Furthermore, we found a correlation (p-value 0.86) between the optically measured fused region and F_{max}. Subsequently, we developed a pulsed phase thermography-based procedure for non-destructively measuring the fused region, resulting in an average difference of approximately 4 % compared to optical measurements. An empirical linear relationship was derived to correlate the welded area obtained by thermal data with F_{max}, enabling the estimation of mechanical joint strength through non-destructive pulsed thermography. This research offers a promising approach for assessing the mechanical integrity of RPW joints using thermal imaging techniques.

Introduction

As of today, one of the primary objectives in industrial research within the transportation sector is undeniably the pursuit of vehicle lightweighting to achieve significant environmental benefits, such as reduced fuel consumption. In pursuing this goal, the adoption of joining technologies plays a pivotal role, notwithstanding several inherent limitations associated primarily with welding processes. The assessment of welded joint quality, coupled with their design, constitutes a formidable challenge in mechanical engineering. Given the intricacies of the welding process, welded joints typically represent critical elements requiring meticulous assessment through non-destructive testing methodologies (Pouranvari and Marashi, 2013, Gould, 2023; Summerville et al., 2017; Hao et al., 1996; Vértesy and Tomáš, 2018; Zhao et al., 2020; Palumbo et al., 2019; Köhler et al., 2022; Walther et al., 2022).

Conventionally, the most prevalent non-destructive testing methods for welded joints encompass surface techniques, including liquid penetrant and magnetic particle testing and volumetric methods, with ultrasonic testing (UT) and X-rays being the most widely employed (Pouranvari and Marashi, 2013, Gould, 2023; Summerville et al., 2017; Vértesy and Tomáš, 2018; Jonietz et al., 2016; Kastner et al., 2021; Moghanizadeh, 2016; Hua et al., 2019; Thornton et al., 2012). However, these methods, renowned for their robustness and versatility, have limitations. They often necessitate direct contact with the component or surface treatments, exhibit timeframes incongruent with industrial production, and pose challenges in terms of automation (Summerville et al., 2017; Battaglini et al., 2015; Provencal and WeldNet, 2022; Cruz et al., 2017). Moreover, they encounter difficulties when applied to very thin joints, which are frequently of paramount interest in the automotive context for the abovementioned reasons (Guo, 2020; Dell'Avvocato et al., 2022; Dell'Avvocato et al., 2021).

Amongst the welding techniques commonly employed for thin joints, resistance welding holds extensive utility across various industrial sectors, with the automotive industry at the forefront. These welds, especially prevalent in components such as the body frame, are utilised not only for structural purposes but also for aesthetic components subsequently subjected to painting (Dell'Avvocato et al., 2022; Dell'Avvocato et al., 2021; Nielsen et al., 2015; Yetilmezsoy et al., 2018; Müller et al., 2023; Kimura et al., 2022; Faye et al., 2021; Wang and Zhang, 2017).

The most prevalent form of resistance welding is resistance spot welding (RSW), achieved by applying force through two electrodes, thereby permitting current flow for several seconds, inducing localised

* Corresponding author.
E-mail address: giuseppe.dellavvocato@poliba.it (G. Dell'Avvocato).

https://doi.org/10.1016/j.jajp.2023.100177

Available online 15 December 2023

temperature elevation that results in material fusion and typically yields a circular joint due to the force exerted on the two plates (Summerville et al., 2017; Hao et al., 1996; Zhao et al., 2020; Palumbo et al., 2019; Jonietz et al., 2016; Kastner et al., 2021; Hua et al., 2019; Thornton et al., 2012; Martín et al., 2007).

A noteworthy innovation in resistance welding technology, which we examined in this study, is Resistance Projection Welding (RPW) (Dell'Avvocato et al., 2022; Dell'Avvocato et al., 2021; Nielsen et al., 2015; Yetilmezsoy et al., 2018; Wang and Zhang, 2017; Schwenk and Shearer, 2023; Furlanetto et al., 2012). RPW operates on the same principles as RSW but with a substantial difference: one of the two plates is pre-deformed plastically, creating a raised area or "projection." Consequently, the contact area is significantly reduced, leading to localised temperature elevation, as depicted in Fig. 1. This results in a joint characterised by a rectangular geometry with a smooth front surface and a rear surface where the projection remains visible. Notably, this process offers a principal advantage in not introducing any aesthetic alterations to the front surface, a significant advantage for the aesthetic requirements of automobiles (Dell'Avvocato et al., 2022; Dell'Avvocato et al., 2021; Nielsen et al., 2015; Yetilmezsoy et al., 2018; Wang and Zhang, 2017; Schwenk and Shearer, 2023; Furlanetto et al., 2012). Moreover, from a technological perspective, RPW allows for reduced applied force and the current passage time, transitioning from the order of seconds in RSW to milliseconds in RPW.

As is typical in technological processes, defects may arise that influence the welded joint's final quality and mechanical strength (Provencal and WeldNet, 2022; Ma et al., 2022; Kechida et al., 2008). The characteristic defects are similar for both welding mentioned above types and include issues such as excessively small or large nuggets, material expulsions, voids, cracks, or distortions (Gould, 2023; Wang and Zhang, 2017; Martín et al., 2007; Dahmene et al., 2022; Summerville et al., 2019; Schramkó et al., 2022; Xia et al., 2019). However, distortions are considerably less pronounced in RPW.

To ascertain the quality of resistance spot welds, particularly their final mechanical strength, destructive methods such as the chisel, peeling, or tensile tests are typically employed (Summerville et al., 2017; Palumbo et al., 2019; Summerville et al., 2019). Traditional non-destructive testing methods, such as UT, as previously mentioned, encounter limitations when applied to very thin welds, which are most suitable for this joining process (Gould, 2023; Summerville et al., 2017; Moghanizadeh, 2016; Hua et al., 2019; Thornton et al., 2012; Provencal and WeldNet, 2022; Cruz et al., 2017; Guo, 2020; Müller et al., 2023; Furlanetto et al., 2012; Kechida et al., 2008; Schramkó et al., 2022; Martín et al., 2007). Consequently, active thermography emerges as a promising technique, offering several advantages. It enables whole-field inspection, does not require contact with the component, and features timeframes more compatible with industrial production than ultrasonic or X-ray inspections (Jonietz et al., 2016; Kastner et al., 2021; Guo, 2020; Dell'Avvocato et al., 2022; Dell'Avvocato et al., 2021; Sesana et al., 2023; Schlichting et al., 2012; Santoro et al., 2023).

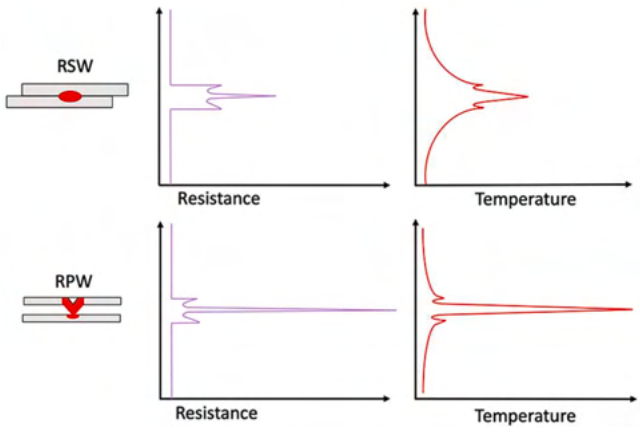

Fig. 1. Qualitative scheme of resistance spot welding and resistance projection welding processes. Qualitative difference of behaviour of temperature and thermal resistance in the plates.

Indeed, this technique has been successfully employed on RSW joints for quantifying the fused area of the joint or detecting internal defects, as well as making qualitative assessments regarding joint suitability (Palumbo et al., 2019; Jonietz et al., 2016; Kastner et al., 2021; Guo, 2020; Dell'Avvocato et al., 2022). However, despite various applications on RSW joints, the literature on non-destructive thermographic inspections remains scarce, and there exist no procedures that account for the non-axisymmetric geometry of the joints, which, in the case of the investigated RPW joints, possess a rectangular geometry as opposed to the traditional circular shape. Preliminary work in this direction has been presented in recent years (Dell'Avvocato et al., 2022; Dell'Avvocato et al., 2021), initially exploring the possibility of linking specific thermographic features to the process parameters (Dell'Avvocato et al., 2021). Subsequently, a preliminary procedure was presented to estimate the welded area in RPW joints through laser thermography, comparing the results with those obtained from UT tests (Dell'Avvocato et al., 2022). Building upon these preliminary works, the present study unfolds.

In this study, we propose a thermographic procedure based on flash thermography and analysed using the Pulse Phase Thermography (PPT) algorithm (Oswald-Tranta, 2016; Oswald-Tranta, 2017; Ibarra-Castanedo and Maldague, 2004; Maldague et al., 2002; Vavilov et al., 1998) to evaluate welded joint quality and estimate its mechanical properties. Specifically, twelve welded joints were produced through the RPW process, utilising four distinct sets of process parameters based on a factorial design. Subsequently, flash thermography tests were conducted, followed by mechanical tests to assess the maximum strength of each joint. The correlation between process parameters and mechanical resistance has been investigated, subsequently developing a thermographic procedure capable of quantitatively measuring the welded area and, through this measurement, estimating the mechanical resistance of the joints.

Materials and methods

Theory

Flash thermography, employed in the present study, is now well-established as a non-destructive testing method for composite (Oswald-Tranta, 2016; Oswald-Tranta, 2017; Ibarra-Castanedo and Maldague, 2004; Shepard et al., 2009; Vavilov and Pawar, 2015; Vavilov and Burleigh, 2015; Moskovchenko et al., 2022; Palumbo et al., 2019; Maierhofer et al., 2018; Müller et al., 2020) and metallic materials (Dell'Avvocato et al., 2021; Sesana et al., 2023; Santoro et al., 2023; Verspeek et al., 2022; D'Accardi et al., 2018; Montinaro et al., 2021; Waugh et al., 2014) with various applications (Laureti et al., 2018; Parker et al., 1961; Salazar et al., 2014; Cernuschi and Bison, 2008). This technique is based on the solution of the heat conduction equation under the assumptions of a Dirac pulse, semi-infinite, isotropic, and homogeneous body, one-dimensional heat flow, and adiabatic process (Vavilov and Pawar, 2015; Vavilov and Burleigh, 2015; Ibarra-Castanedo, 2023). Specifically, a reflection configuration was considered, wherein the temperature distribution on the heated surface is considered, resulting in the relationship (1).

$$T(0,t) = T_0 + \frac{Q}{e\sqrt{\pi t}} \tag{1}$$

In the Eq. (1), T_0 represents the initial surface temperature, Q is the surface energy density, t denotes time, and e signifies thermal effusivity, obtained as the square root of the product of density, thermal conductivity, and specific heat of the material.

As widely known, pulsed active thermography in a reflection configuration involves exciting a surface with a thermal pulse and observing the surface cooling through a thermal camera (Vavilov and Pawar, 2015; Vavilov and Burleigh, 2015; Müller et al., 2020; D'Accardi et al., 2018; Ibarra-Castanedo, 2023). The presence of internal inhomogeneities within the material results in varying thermal responses on the surface between healthy and defective regions. To enhance the signal contrast, several algorithms exist in the literature (Oswald--Tranta, 2016; Oswald-Tranta, 2017; Ibarra-Castanedo and Maldague, 2004; Maldague et al., 2002; Shepard et al., 2009; Vavilov and Burleigh, 2015; D'Accardi et al., 2018), including the pulsed phase thermography employed in this study. This technique involves a shift from time-domain analysis to frequency-domain analysis, enabling the generation of 3D matrices containing phase and amplitude maps as functions of frequencies (Oswald-Tranta, 2016; Oswald-Tranta, 2017; Ibarra-Castanedo and Maldague, 2004; Vavilov et al., 1998; Ibarra--Castanedo, 2023). The frequency f, as described by the relationship (2), correlates with the inspection depth z through thermal diffusivity α.

$$z \propto \sqrt{\frac{\alpha}{\pi f}} \tag{2}$$

Specimens

To assess the impact of process parameters on welding quality, specifically mechanical strength, twelve steel (DC 04 and DC 05 EN 10,130) welded joints were fabricated using the RPW (Resistance Projection Welding) process (Fig. 2). Three primary production parameters were considered: applied force between the electrodes (F), current intensity (I), and the duration for which the current was applied (t). These parameters were systematically varied according to a factorial design, resulting in four distinct set parameters. Three replicates were performed for each of these sets, yielding a total of 12 specimens, with each parameter set repeated three times, as summarized in Table 1.

The two steel plates (DC 04 and DC 05 respectively for embossed and front plate), joined together using RPW, had thicknesses of 0.67 mm (front plate) and 0.70 mm (embossed back plate), as depicted in Fig. 2 b, resulting in a nominal weld joint length of approximately 9 mm (Fig. 3). Fig. 2 c shows that the front surface exhibited no discernible traces of the welding process, making it aesthetically more suitable for automotive applications, particularly in visually prominent areas. Furthermore, unlike RSW, RPW joints displayed a consistently homogeneous surface in terms of surface properties, eliminating issues related to heterogeneous emissivity commonly associated with RSW. Nonetheless, the front

Table 1
Process welding parameters used in manufacturing process and ID code of specimens.

Specimen	Current [kA]	Force [kN]	Time [ms]	Replications
J1_DOE_1	15	1.4	10	3
J1_DOE_2	13	1.4	12	3
J1_DOE_3	13	1.6	10	3
J1_DOE_4	15	1.6	12	3

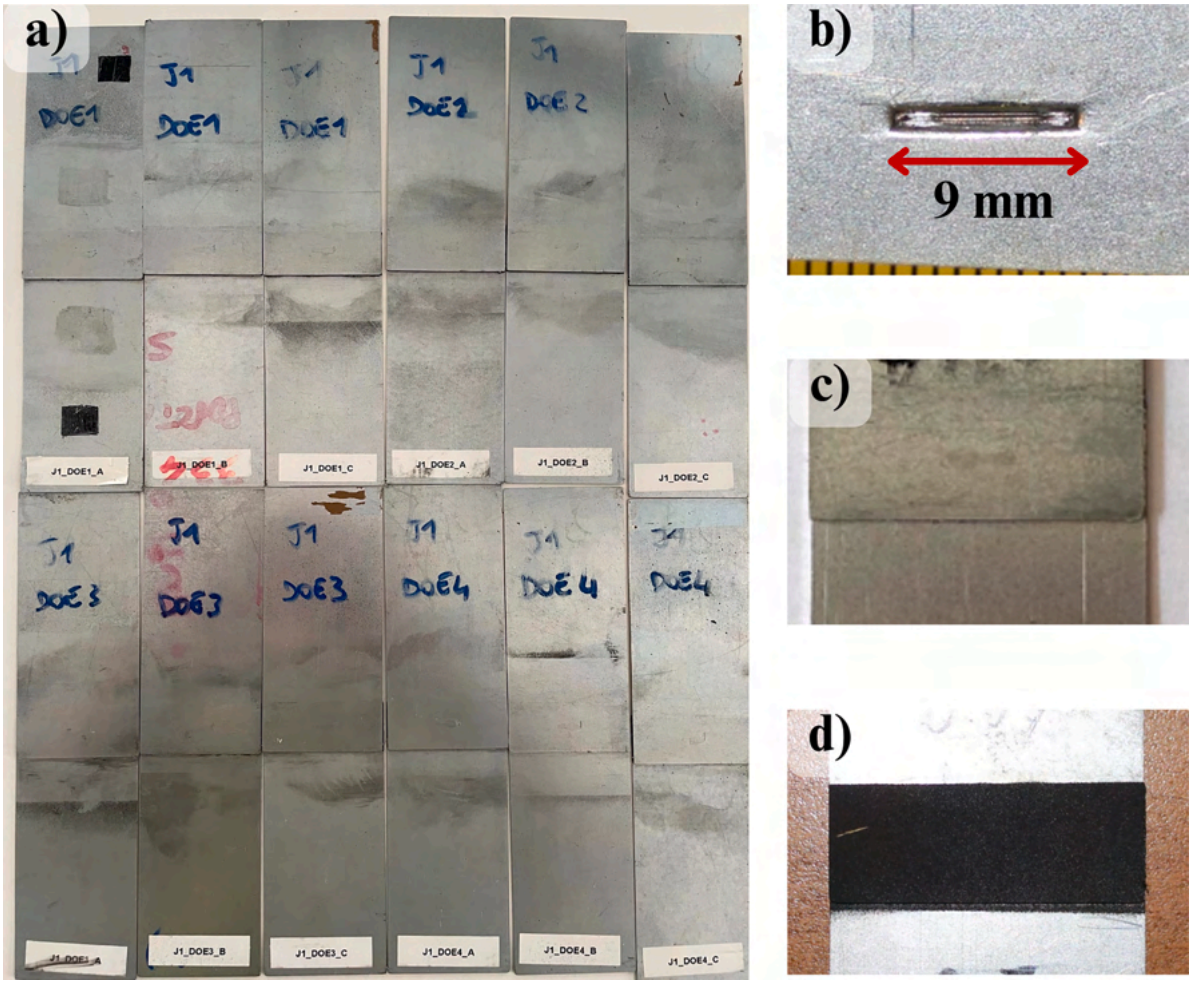

Fig. 2. (a) RPW joints analysed. (b) Rear plate detail with measure of embossing. (c) Front plate with high aesthetical quality. (d) Front plate with black paint to increase absorptivity and emissivity.

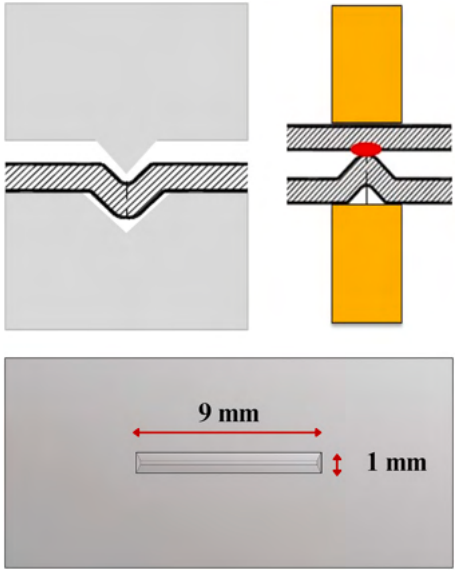

Fig. 3. Scheme of the geometry of welded plates and process steps.

surface was coated with a high-emissivity black paint (emissivity of 0.98) to enhance surface emissivity and absorption for inspection purposes, as in its natural state, it possesses a reflective surface despite its homogeneity (Fig. 2 d).

Experimental setup

Given the geometry of the inspected joints, which exhibited a pronounced geometric variation on the rear face, a reflection setup was preferred, meaning that the heat source was positioned on the same side as the observed surface. The front surface of the specimen was observed using a FLIR X6540sc thermal camera after heating for approximately 3 ms by employing two 3 kJ x 2 flash lamps placed symmetrically on either side of the IR camera, which was positioned in front of the welded joint (Fig. 4). The duration of the heating has been approximately evaluated considering the heating part of curve obtained from thermographic results, which confirms the estimated value given by the producers.

For each test, a sequence involving surface heating and cooling was recorded at 910 Hz, lasting a total of 4 s. A -10 to 55 °C calibration range was set with an acquisition window width of 304 × 104 pixels^2 obtaining 0.055 mm/pxl, enabling such a high acquisition frequency. The thermal imaging setup used is illustrated in the figures below, with its architecture summarized in Fig. 5.

Mechanical tests were carried out using an MTS Model 370 Load Frame with a load cell capacity of +/- 100 kN at a 1 mm/min rate. To ensure load application along the central axis, considering the imperfect symmetry of the plates (single lap joint), the terminal region of each of the two welded plates was removed and used as a spacer between the welded plate and the grip of the testing machine, thus ensuring symmetry, avoiding any spurious bending. The tests were performed by applying a tensile load to the two plates, however, given the geometry of the analysed welded area, it should be noted that the stress state is certainly triaxial. For this reason, the maximum force required to fracture the welded joint will be considered as the output for the mechanical tests.

Methods

The thermographic tests were carried out following the setup described in the preceding section. Each test underwent three repetitions to ensure measurement repeatability. After the thermographic evaluations, destructive mechanical tests have been conducted. As previously outlined, to mitigate misalignment concerns during the mechanical tests, spacers fashioned from one of the plates were employed. These mechanical tests aimed to determine each specimen's maximum force (F_{max}). The outcomes of these tests were subjected to ANOVA analysis to gauge the impact of welding process parameters on the final mechanical strength.

Subsequently, given the limited deformation that has been observed in the joints post-mechanical testing, we examined the weld fusion zone using low-magnification photography for each specimen. This allowed us to measure the fusion zone's area and shape in each weld. The fusion zone data acquired through this procedure was treated as an output and index directly correlated to the tensile strength of the joints. In this regard, an ANOVA analysis was performed to ascertain whether the fusion zone area exhibited sensitivity to the same parameters that influenced the measured F_{max}. Upon confirmation, we established a statistical correlation between the fusion zone measurements obtained through optical methods and the maximum force recorded in the mechanical tests.

Next, we devised an analytical procedure for the thermographic tests conducted before specimen fracture. As mentioned in previous sections, we adopted the Pulsed Phase Thermography (PPT) algorithm for analysis. While this algorithm typically provides amplitude and phase maps, this study focused on the phase maps due to their reduced noise levels and the additional information they offer compared to thermal maps (Dell'Avvocato et al., 2022; Vavilov and Pawar, 2015; Vavilov, 2004).

To undertake a quantitative analysis of the fusion zone, we needed to determine the most suitable frequency for evaluating the corresponding phase map. The frequency selection process involved proposing and applying a procedure to a single specimen (J1_DOE1_A). This procedure encompassed extracting the recorded sequence of temperature maps (Fig. 6 a), subtracting the cold frame (Fig. 6 b), and employing the Fast

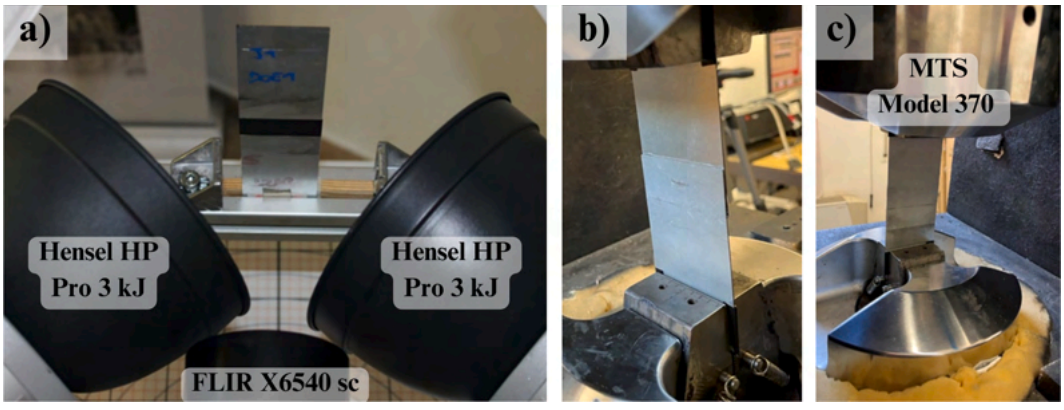

Fig. 4. (a) Reflection mode experimental thermographic set-up adopted. (b, c) Experimental set-up for destructive test and measurement of F_{max}.

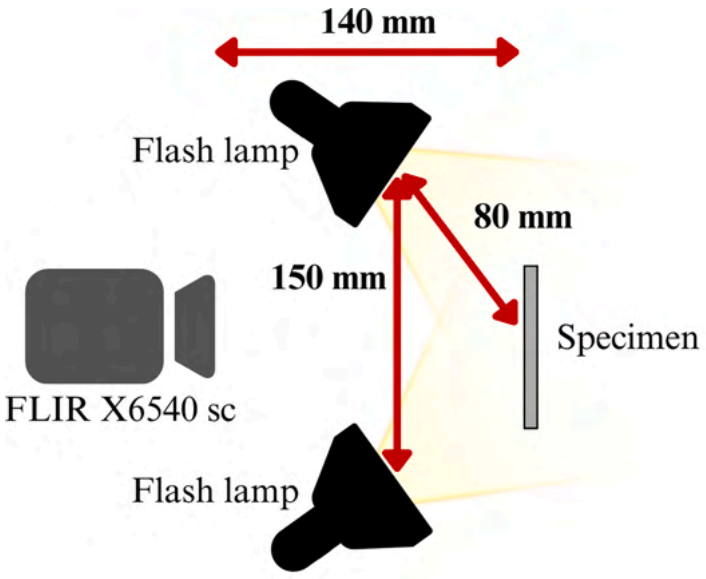

Fig. 5. Scheme of architecture of the experimental set-up.

Fourier Transform (FFT) (Plonka et al., 2018) for signal analysis in the frequency domain. Notably, only phase maps were considered (Fig. 6 c). Within the phase map matrix, a non-welded region measuring 10 × 10 pixels^2 was identified for each frequency as showed in Fig. 6 a. For each phase map, thus for each frequency (f), a 10 × 10 pixel^2 region corresponding to a certainly non-welded area, defined as the "sound area", was identified (red square Fig. 6 a). Subsequently, the mean phase value in this Region of Interest (ROI) was determined by calculating the average phase value, denoted as $P_{f,sound}$. For each pixel (i,j), in each phase map (f), the phase value ($P_{f,\,i}$) was considered, and the mean value for the sound region in the same phase map ($P_{f,sound}$) was subtracted from it to obtain the phase contrast. To achieve normalization with respect to background noise, the standard deviation of the signal in the identified ROI for the healthy region was calculated, which is indicative of the background noise ($\sigma_{f\mathbf{sound}}$). The previously obtained phase contrast was then divided by this value, providing a quantitative indication of how many times the contrast exceeds the background noise, as indicated in relation (3). In Fig. 6 d there is an example of an NPC map.

$$NPC = \frac{P_{f,i,j} - P_{f,sound}}{\sigma_{f,sound}} \tag{3}$$

To facilitate differentiation between the welded and non-welded regions, we established a threshold value akin to prior studies in the literature[19,53,61]. A threshold value of -2 for the phase contrast was deemed appropriate, as it indicates a signal at least twice the standard deviation of the noise, effectively distinguishing the welded region from the non-welded one. Each phase map in the matrix was segmented using this threshold value, with minor discontinuities stemming from signal noise being addressed using the *imfill(BW, 'holes')* command in MATLAB®. This process ensured uniformity in the area derived from the thermographic tests.

Subsequently, we counted the number of pixels representing the welded zone (assigned a value of 1) for each normalised phase contrast map at every frequency. These pixel counts were converted to mm^2 per pixel, yielding total measurements of the welded area for each phase map. This process generated 2100 area values, each corresponding to a specific frequency.

We compared each obtained area value with the optical measurement for J1_DOE1_A to identify the inspection frequency, calculating the absolute percentage difference as reported in Fig. 7. Plotting the curve of the percentage difference between thermographic and optical measured areas against the frequencies enabled us to select the frequency at which the difference between these measurements was minimised for the remaining eleven specimens. It is worth to underline that we can consider always the same frequency for all the joints because the nominal thickness of the plate does not change. This selection was justified by the uniform nominal thickness of the plates and the correlation between thermal signal frequency and inspection depth, suggesting that the frequency-minimising measurement error on the welded area was consistent.

The procedure for frequency selection above described is summarised in Fig. 8. For the remaining eleven specimens, the same procedure was applied to obtain the phase map matrix. Subsequently, steps 4 to 7 (Fig. 8) were repeated solely for the frequency defined through the preceding procedure.

The values obtained for the welded region were subjected to statistical analysis to evaluate the influence of welding process parameters and their correlation with the F_{max} values obtained from destructive tests. ImageJ® software was employed for analising photographic images of the fracture surface to measure the welded region after destructive tests. The melted area was visually identified, and its boundaries were manually traced. Then, through the software tools, the sum of the melted area was calculated. This method introduces uncertainty due to the visual approach, primarily associated with the operator.

Ultimately, an empirical relationship between measured area with the thermal method and mechanical joint strength was established, allowing for non-destructive evaluation.

Specifying that the welded region's area is not the sole parameter influencing the final mechanical strength is essential. Besides the welded area distribution, the microstructure of the region and surrounding metallurgical properties can also play a significant role. However, these factors depend on the thermal cycles occurring during welding, thus influenced by process parameters. Consequently, these thermal effects have been indirectly considered in evaluating the impact of time and current process parameters on the joint's final mechanical strength.

Results and discussion

Fig. 9 displays the results of F_{max} obtained from the mechanical strength tests. On the x-axis, the combinations of process parameters can be observed (DOE 1/2/3/4), while the y-axis represents the values of the maximum force measured for each replication (DOE n A/B/C). A qualitative assessment reveals good repeatability amongst the specimens,

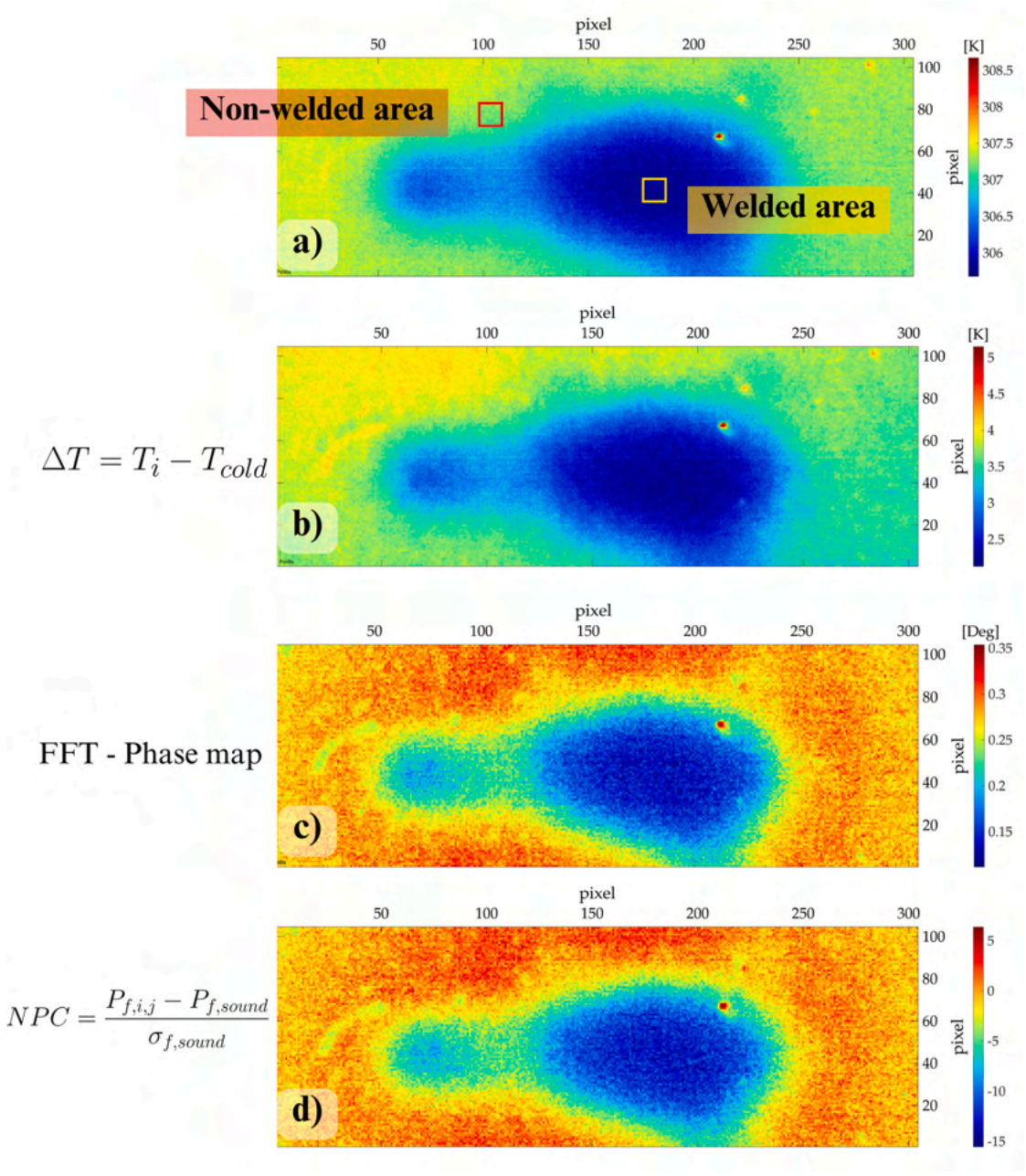

Fig. 6. (a) Example of a thermal map for J1_DOE1_A highlighted the non-welded and welded areas considered. (b) The corresponding map in a) but with subtraction of cold frame. (c) an Example of a phase map after the PPT algorithm application, and (d) the corresponding normalised phase contrast map.

with reasonably low standard deviations for most of them, except for DOE 2, which exhibits the highest dispersion. The higher dispersion can be attributed to instability in the welding process with the DOE 2 parameter set. It is crucial to note that not necessarily all the utilised process parameter sets are optimal, a determination that requires a comprehensive optimisation of the production process. However, this is beyond the scope of the current study, which focuses on a comparative evaluation of the employed parameter sets.

Based on the ANOVA results concerning the relationship between process parameters and F_{max}, it became evident that F_{max} values were primarily influenced by the duration of current application between the electrodes and the force applied during the process. In contrast, the current applied between the electrodes appeared to have negligible impact compared to the other two parameters, as summarised in the Pareto chart in Fig. 10.

Consequently, it can be deduced that for ensuring a specific mechanical strength of the final joint the critical parameters to control are the duration (t) and force (F), as variations in these parameters during the process would lead to significant variations in the final mechanical strength (F_{max}).

As described in the previous section, post-destructive tests, all specimens were analysed to assess the fusion zone for each of them. Fig. 11 presents images of the welded joints after fracture, while Table 2 lists the values of the fusion zone measured as described. It is noticeable that, in some cases, there is a discontinuity within the fusion zone compared to the expected geometry. An asymmetry in the joint concerning the transverse axis is apparent. This asymmetry may be attributed to imperfect electrode contact, appearing as either a break in the welding region or one side being wider than the other. Consequently, the electric arc that leads to material fusion may not occur simultaneously along the entire length, resulting in an uneven temperature distribution. In cases of discontinuity, it was, understandably, excluded from the

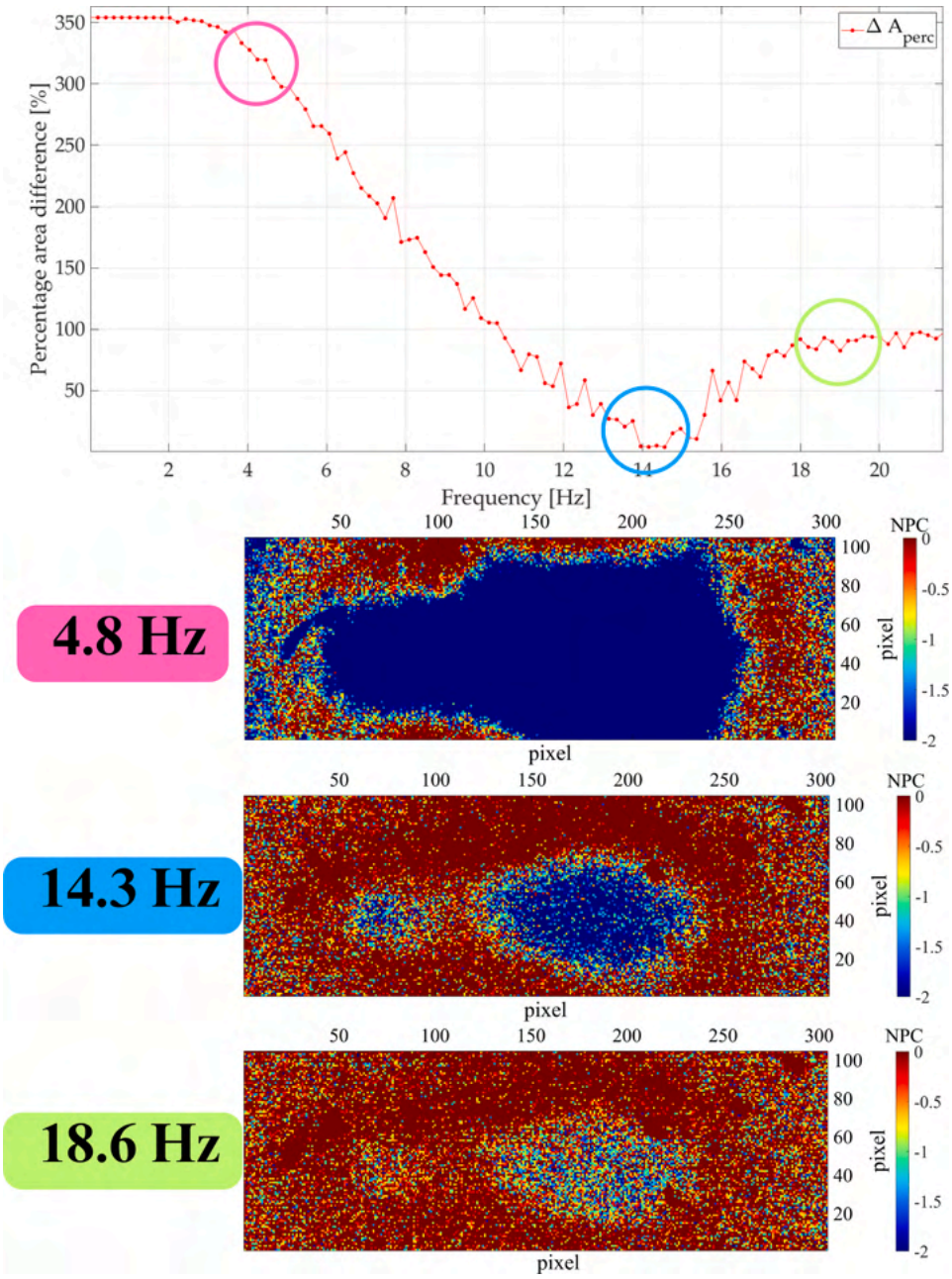

Fig. 7. The trend of percentage error between thermographic and optical area as a function of frequencies for J1_DOE1_A. Examples of Normalized Phase Contrast maps in different parts of the curve: (pink) before the minimum, (light blue) at the minimum and (green) after the minimum.

assessment of the total welded area. An ANOVA analysis was conducted to evaluate the influence of process parameters on the measured fusion zone, and the corresponding Pareto chart is shown in Fig. 10 b. It can be observed that the measured total area value is primarily dependent on process parameters such as duration (t) and force (F), precisely like the F_{max} measured in the previous mechanical tests.

From these results, it can be deduced that the welded area can be a good indicator of weld strength. Therefore, we assessed the correlation between the F_{max} and the area measured with optical methods, yielding a Pearson correlation coefficient of 0.86 and a P-value less than 0.001, which statistically confirmed the correlation between the two quantities. On the other hand, to evaluate the potential effect of welding discontinuity on the detected F_{max}, a statistical analysis was carried out for investigating the correlation between these two variables, yielding a negative outcome. This demonstrated the insignificance of the extent of the discontinuous area on the mechanical strength of the joint, with a Pearson coefficient of -0.39, indicating a lack of correlation.

The thermographic procedure outlined in Fig. 8 and described in 2.4 resulted in obtaining a curve representing the percentage error of the total area value as a function of frequency for specimen J1_DOE1_A. As expected, this curve has a minimum point, as depicted in Fig. 12, corresponding to a frequency of 14.3 Hz. Subsequently, we obtained the total fused area values for each of the remaining welds by considering the threshold value for the normalised phase contrast and the obtained frequency, as summarised in Table 2. The measurements of the welded areas obtained through the thermographic procedure exhibited relatively small differences compared to those measured with optical methods. The mean percentage error obtained is approximately 4 %, with a maximum of around 7 %. These values can be considered acceptable for the type of inspection, considering that the differences are about 1.2 mm^2. It is important to highlight that in most cases, the thermographic procedure tended to overestimate the welded area,

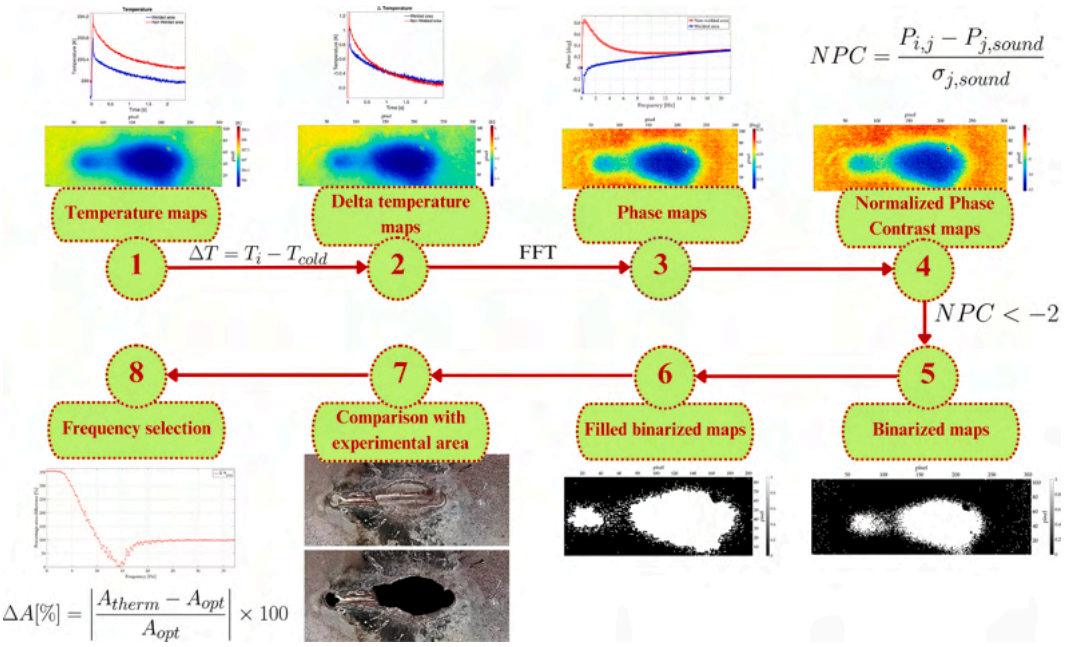

Fig. 8. Scheme of the thermographic procedure proposed and adopted for frequency selection.

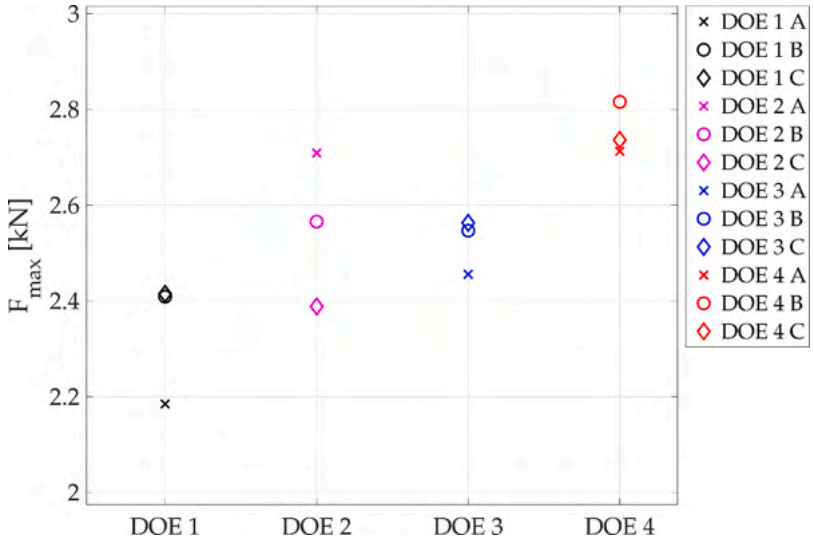

Fig. 9. Values of F_{max} obtained for each set of parameters (black-pink-blue-red) and for each repetition (cross-circle-diamond).

posing a risk of considering a plate adequately welded when it may not be. In fact, this error can depend on the expulsion of the material close to the edges of the welded area, which is difficult to predict but can generate the overestimation of the error. Another source of this error can be the not perfectly constant depth of embossing, thus the not exactly constant value of the global thickness of the welded joint in the welded area that can be influenced slightly by the process parameters. This slight change in the plates interface depth can result in a shift of the frequency for which the error is minimal, resulting in an overestimation of the welded area too. However, this error is not systematic, making it challenging to correct.

Another ANOVA was carried out to verify the correlation between mechanical resistance and the area measured by thermographic data. The results confirmed the dependency of the thermographically measured area on process parameters such as duration and force applied to the electrodes. The correlation between F_{max} and the thermographic area exhibited a Pearson coefficient of 0.84 and a P-value of approximately 0.001. Furthermore, this correlation is visually represented in Fig. 13, which displays the thermographically measured area values, including repetitions, corresponding to their respective F_{max} values. With a reasonable approximation, a linear correlation can be used to plot the data in the graph, and this is confirmed by an R-squared value of 0.96, indicating the adequacy of the adopted model to describe this relationship.

The resulting empirical model, established for joints with the current geometry, estimates the mechanical properties of the welded joint. This estimation can be made non-destructively by measuring the welded area through flash thermography.

In Fig. 14, four of the twelve joints were compared in terms of thermographic method versus optical images of the fused region after mechanical testing. The thermographic technique can detect discontinuities within the welded area, as observed in the DOE 1 and four comparisons. This indicates the potential to identify internal welding defects such as material expulsion and incomplete fusion.

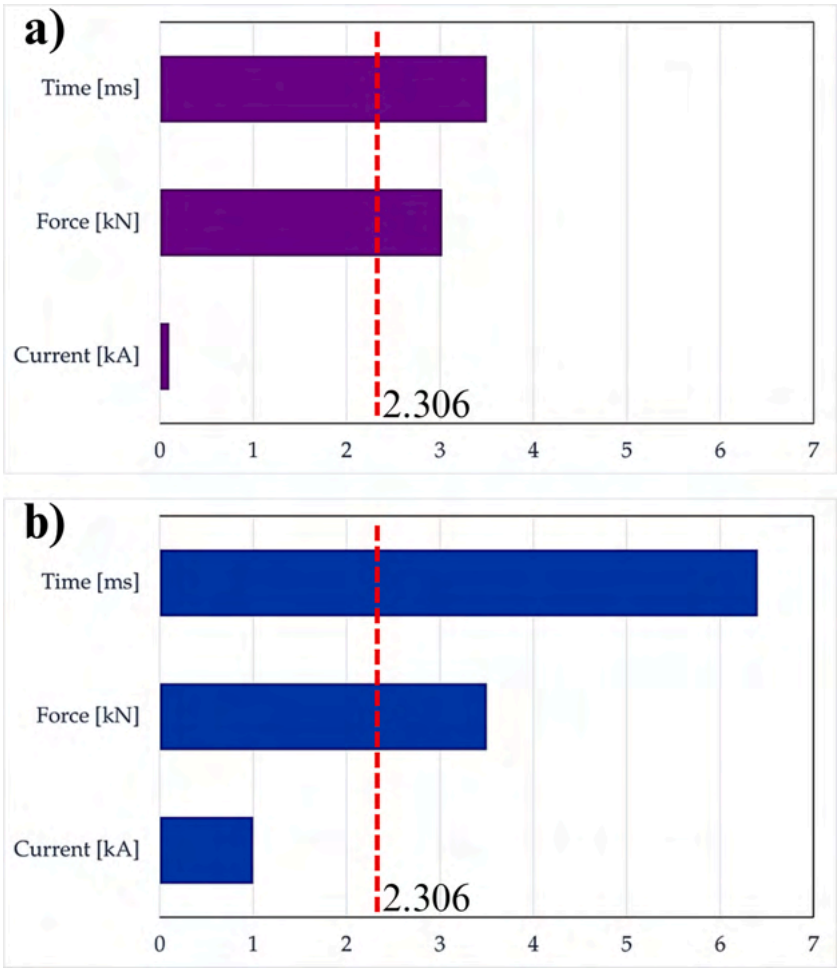

Fig. 10. (a) Pareto chart obtained for process parameters vs F_{max}. (b) Pareto chart obtained for process parameters vs A_{opt}.

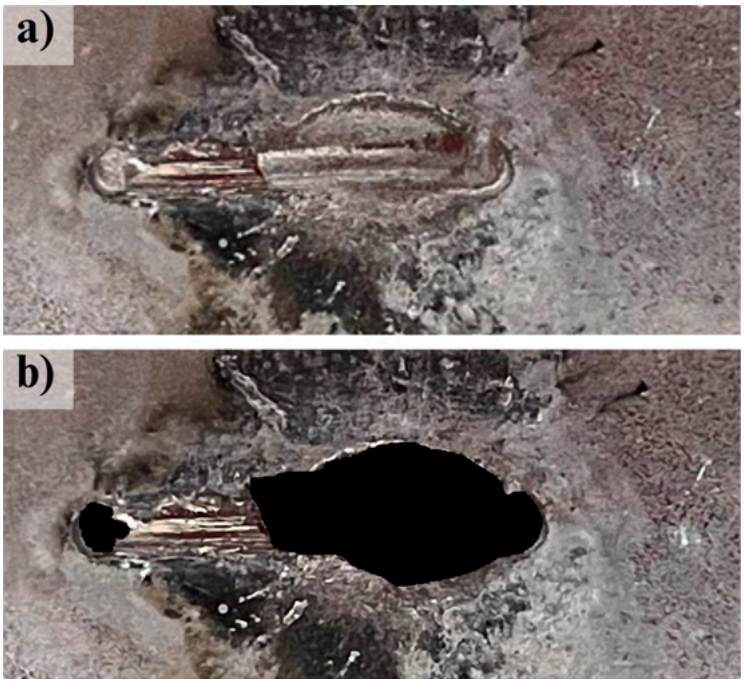

Fig. 11. (a) Optical image and (b) example of measurement of welded area for the DOE_1_A.

Table 2
Results obtained from optical measurement and thermographic ones at frequency of 14.3 Hz. In the last column the percentage difference between optical and thermographic value of welded area measured.

Specimen	Repetition	Frequency [Hz]	A_{opt} [mm^2]	A_{therm} [mm^2]	Difference [%]
J1_DOE_1_A	3	14.3	11.55	11.68 ±0.16	1.4
J1_DOE_1_B	3	14.3	13.59	13.15 ± 0.41	3.4
J1_DOE_1_C	3	14.3	14.86	15.03 ± 0.07	1.1
J1_DOE_2_A	3	14.3	17.60	17.56 ± 0.12	0.5
J1_DOE_2_B	3	14.3	16.62	16.44 ± 0.88	4.5
J1_DOE_2_C	3	14.3	17.37	17.40 ± 1.64	7.4
J1_DOE_3_A	3	14.3	15.63	15.16 ± 0.76	4.6
J1_DOE_3_B	3	14.3	15.77	15.66 ± 0.34	1.5
J1_DOE_3_C	3	14.3	15.51	15.31 ± 0.19	1.3
J1_DOE_4_A	3	14.3	18.43	18.16 ± 0.34	1.9
J1_DOE_4_B	3	14.3	18.02	17.87 ± 1.02	4.6
J1_DOE_4_C	3	14.3	18.81	18.84 ± 0.63	2.4

Conclusions

In this study, twelve welded joints were analysed using Resistance Projection Welding (RPW) with two primary objectives: to investigate the influence of process parameters on the mechanical strength of the joints and to develop a thermographic procedure based on flash thermography capable of non-destructively estimating the mechanical strength of these joints.

Mechanical strength tests were conducted on specimens with varying process parameters, identified through ANOVA. The fused area, optically measured after destructive tests, correlated significantly with strength. A Pulse Phase Thermography (PPT) thermographic procedure was developed, segmenting images with a literature-established threshold. The welded area measured through thermography was compared with optical measurements to determine the analysis frequency for other specimens.

The described thermographic procedure was applied to all remaining specimens, providing fused area values with an average error of approximately 4 % and a maximum error of around 7 %. The correlation of these values with F_{max} was confirmed, allowing for the proposal of an empirical law for estimating mechanical strength in this type of joint by measuring the fused area.

It was found that the mechanical strength of RPW joints primarily depends on the force applied between the electrodes and the process duration. Furthermore, it was demonstrated that flash thermography is a valid method for non-destructively assessing the quality and mechanical strength of RPW joints through the proposed empirical law, which enables the estimation of F_{max} by measuring the fused area.

Despite numerous advantages over traditional methods currently in use, the proposed procedure has limitations. Firstly, the fused area value tends to be overestimated, potentially leading to a type II error by incorrectly classifying an area as welded when it may not meet the threshold criteria. Another limitation is the requirement for specimen coating, which can be overcome by using higher energy densities, representing a future development in this work. Additionally, future outlooks include:

- increasing the pulse duration with different heating source to simplify instrumentation;
- testing the procedure on different thicknesses;
- comparing results from different algorithms to evaluate which minimises measurement error and computational workload most effectively.
- using deep learning for analysing thermal data and automatically detecting the welded area.

Funding

This research received no external funding.

CRediT authorship contribution statement

G. Dell'Avvocato: Conceptualization, Data curation, Formal analysis, Investigation, Methodology, Writing – original draft. **D. Palumbo:** Funding acquisition, Project administration, Resources, Supervision,

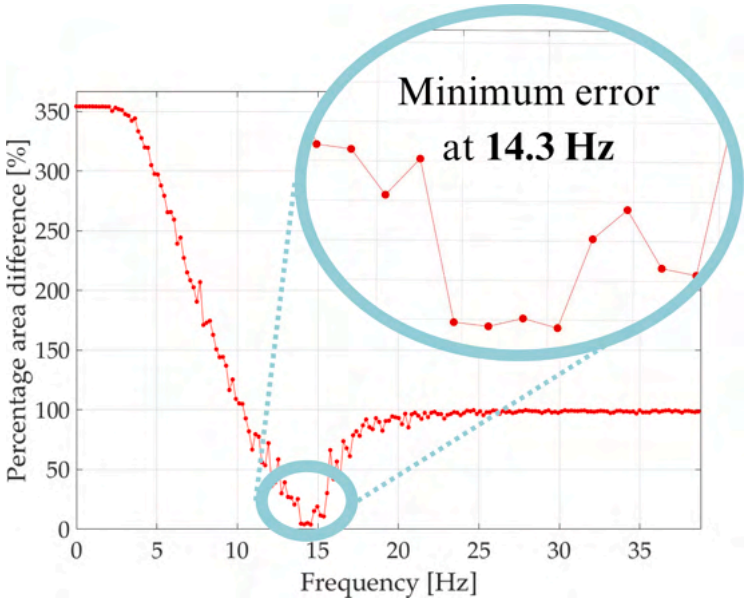

Fig. 12. Plot of percentage difference between optical area and thermographic area as function of frequency for the DOE_1_A specimen.

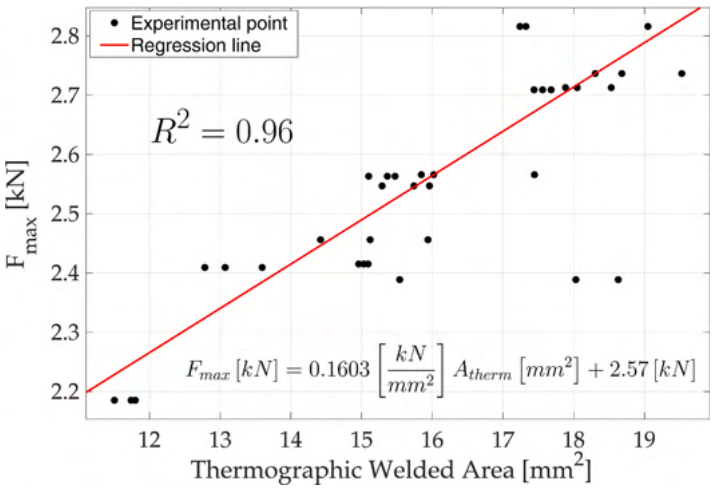

Fig. 13. F_{max} measured through destructive method as function of welded area measured by thermographic procedure proposed. The black dots are the experimental measurements, and the red line represents the regression line with the empirical law in lower part of figure.

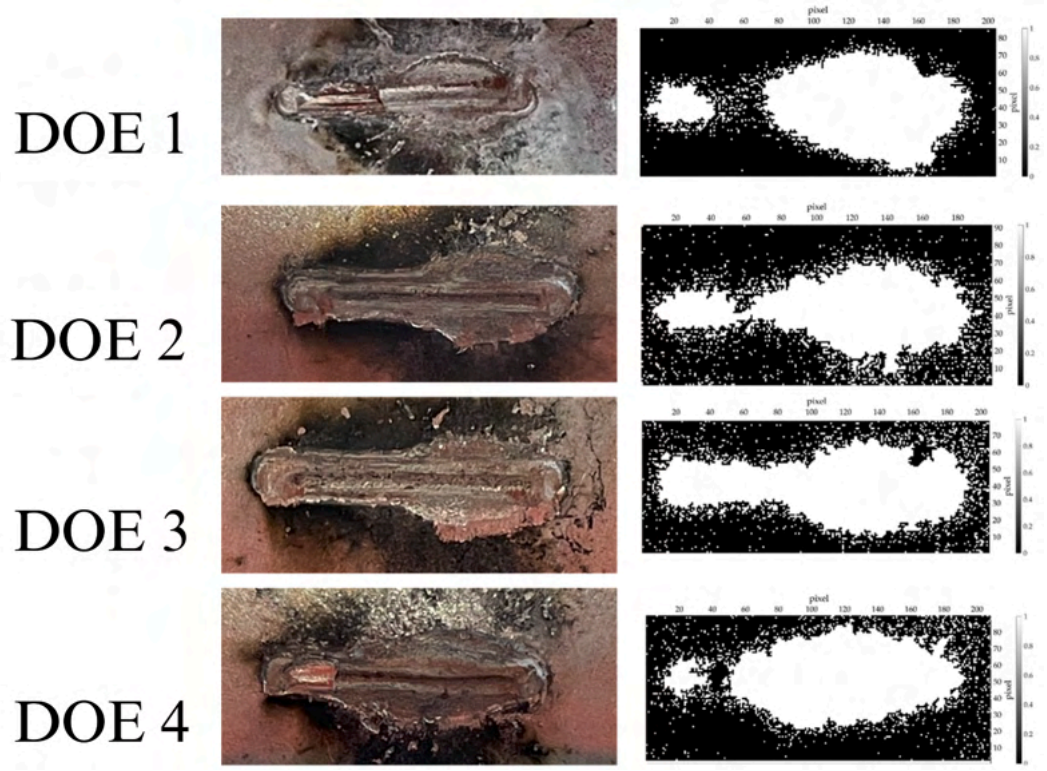

Fig. 14. Qualitative comparison between optical image and thermographic welded area obtained by developed procedure.

Writing – review & editing.

Declaration of Competing Interest

The authors declare that they have no known competing financial interests or personal relationships that could have appeared to influence the work reported in this paper.

Data availability

Data will be made available on request.

References

Battaglini, L., Callegari, S., Caporale, S., Davis, L.A.J., Laureti, S., Senni, L., et al., 2015. Industrial applications of noncontact ultrasonics techniques. Ultrasonic Nondestructive Evaluation Systems: Industrial Application Issues. Springer International Publishing, pp. 271–295. https://doi.org/10.1007/978-3-319-10566-6_11.

Cernuschi, F., Bison, P., 2008. The influence of the laser energy on the thermal diffusivity evaluation of TBC by Laser Flash. J. Therm. Spray Technol. 17, 465–472. https://doi.org/10.1007/s11666-008-9199-8.

Cruz, F.C., Simas Filho, E.F., Albuquerque, M.C.S., Silva, I.C., Farias, C.T.T., Gouvêa, L.L., 2017. Efficient feature selection for neural network based detection of flaws in steel welded joints using ultrasound testing. Ultrasonics 73, 1–8. https://doi.org/10.1016/j.ultras.2016.08.017.

D'Accardi, E., Palumbo, D., Tamborrino, R., Galietti, U., 2018. A quantitative comparison among different algorithms for defects detection on aluminum with the

pulsed thermography technique. Metals 8. https://doi.org/10.3390/met8100859 (Basel).
Dahmene, F., Yaacoubi, S., El, M.M., Bouzenad, A.E., Rabaey, P., Masmoudi, M., et al., 2022. On the nondestructive testing and monitoring of cracks in resistance spot welds: recent gained experience. Weld. World 66, 629–641. https://doi.org/10.1007/s40194-022-01249-w.
Dell'Avvocato, G., Gohlke, D., Palumbo, D., Krankenhagen, R., Galietti, U., 2022. Quantitative evaluation of the welded area in Resistance Projection Welded (RPW) thin joints by pulsed laser thermography. In: Avdelidis, N.P., Mendioroz, A. (Eds.), Thermosense: Thermal Infrared Applications XLIV. SPIE, p. 26. https://doi.org/10.1117/12.2618806.
Dell'Avvocato, G., Palumbo, D., Pepe, R., Galietti, U., 2021. Non-destructive evaluation of resistance projection welded joints (RPW) by flash thermography. IOP Conf. Ser. Mater. Sci. Eng. 1038, 012003 https://doi.org/10.1088/1757-899x/1038/1/012003.
Faye, A., Balcaen, Y., Lacroix, L., Alexis, J., 2021. Effects of welding parameters on the microstructure and mechanical properties of the AA6061 aluminium alloy joined by a Yb: YAG laser beam. J. Adv. Join. Process. 3 https://doi.org/10.1016/j.jajp.2021.100047.
Furlanetto V., Stocco D., Batalha G.F., Szabados F.R. Inspection of projection welded automotive nuts through b-scan ultrasonic acoustic imaging. 2012.
Gould J.E. Vehicle Lightweighting and the Need for Aluminum in Body-in-White Construction Joining Aluminum Sheet in the Automotive Industry-A 30 Year History Resistance welding, mechanical fasteners, and ultrasonic welding are examined in this overview of joining technology, KEYWORDS Aluminum Alloys Body-in-White Resistance Welding Mechanical Fastening Ultrasonic Welding. 2023.
Guo, X., 2020. Ultrasonic infrared thermography of aluminium thin plates for crack inspection in friction stir welded joints. IEEE Sens. J. 20, 6524–6531. https://doi.org/10.1109/JSEN.2020.2976144.
Hao M., Osman K.A., Boomer D.R., Newton C.J. Sponsored by the American welding society and the welding research council developments in characterization of resistance spot welding of aluminum a monitoring system analyzes data and correlates the information to parameters for spot welding aluminum. 1996.
Hua, L., Wang, B., Wang, X., He, X., Guan, S., 2019. *In-situ* ultrasonic detection of resistance spot welding quality using embedded probe. J. Mater. Process. Technol. 267, 205–214. https://doi.org/10.1016/j.jmatprotec.2018.12.008.
Ibarra-Castanedo C. Quantitative subsurface defect evaluation by pulsed phase thermography: depth retrieval with the phase. 2023.
Ibarra-Castanedo, C., Maldague, X., 2004. Pulsed phase thermography reviewed. Quant. InfraRed Thermogr. J. 1, 47–70. https://doi.org/10.3166/qirt.1.47-70.
Jonietz, F., Myrach, P., Suwala, H., Ziegler, M., 2016. Examination of spot welded joints with active thermography. J. Nondestruct. Eval. 35, 1–14. https://doi.org/10.1007/s10921-015-0318-4.
Kastner, L., Ahmadi, S., Jonietz, F., Jung, P., Caire, G., Ziegler, M., et al., 2021. Classification of spot-welded joints in laser thermography data using convolutional neural networks. IEEE Access 9, 48303–48312. https://doi.org/10.1109/ACCESS.2021.3063672.
Kechida, A., Drai, R., Benammar, A., 2008. Image processing and wavelets transform for sizing of weld defects using ultrasonic TOFD images. In: Proceedings of the European Conference on Noise Control, pp. 609–614. https://doi.org/10.1121/1.2932898.
Kimura, M., Sano, Y., Kusaka, M., Kaizu, K., 2022. Methods for improving joint strength of friction stud welded AA5083 alloy joints. J. Adv. Join. Process. 5 https://doi.org/10.1016/j.jajp.2021.100075.
Köhler, D., Sadeghian, B., Troschitz, J., Kupfer, R., Gude, M., Brosius, A., 2022. Characterisation of lateral offsets in clinch points with computed tomography and transient dynamic analysis. J. Adv. Join. Process. 5 https://doi.org/10.1016/j.jajp.2021.100089.
Laureti, S., Sfarra, S., Malekmohammadi, H., Burrascano, P., Hutchins, D.A., Senni, L., et al., 2018. The use of pulse-compression thermography for detecting defects in paintings. NDT E Int. 98, 147–154. https://doi.org/10.1016/j.ndteint.2018.05.003.
Ma, N., Gao, X., Tian, M., Wang, C., Zhang, Y., Gao, P.P., 2022. Magneto-optical imaging of arbitrarily distributed defects in welds under combined magnetic field. Metals 12. https://doi.org/10.3390/met12061055 (Basel).
Maierhofer, C., Krankenhagen, R., Röllig, M., Heckel, T., Brackrock, D., Gaal, M., 2018. Quantification of Impact Damages in CFRP and GFRP Structures with Thermography and Ultrasonics. QIRT Council. https://doi.org/10.21611/qirt.2018.126.
Maldague, X., Galmiche, F., Ziadi, A., 2002. Advances in pulsed phase thermography.
Martín, O., López, M., Martín, F., 2007. Artificial neural networks for quality control by ultrasonic testing in resistance spot weldingOscar. J. Mater. Process. Technol. 183, 226–233. https://doi.org/10.1016/j.jmatprotec.2006.10.011O.
Moghanizadeh, A., 2016. Evaluation of the physical properties of spot welding using ultrasonic testing. Int. J. Adv. Manuf. Technol. 85, 535–545. https://doi.org/10.1007/s00170-015-7952-y.
Montinaro, N., Cerniglia, D., Pitarresi, G., 2021. Laser thermography NDT for the inspection of debonding in titanium based Fibre Metal Laminates. IOP Conf. Ser. Mater. Sci. Eng. 1038, 012045 https://doi.org/10.1088/1757-899x/1038/1/012045.
Moskovchenko, A., Švantner, M., Vavilov, V., Chulkov, A., 2022. Analyzing probability of detection as a function of defect size and depth in pulsed IR thermography. NDT E Int. 130 https://doi.org/10.1016/j.ndteint.2022.102673.
Müller, F.W., Mirz, C., Weil, S., Schiebahn, A., Corves, B., Reisgen, U., 2023. Weld quality characterization by vibration analysis for ultrasonic metal welding processes. J. Adv. Join. Process. 8 https://doi.org/10.1016/j.jajp.2023.100149.
Müller, J.P., Dell'Avvocato, G., Krankenhagen, R., 2020. Assessing overload-induced delaminations in glass fiber reinforced polymers by its geometry and thermal resistance. NDT E Int. 116 https://doi.org/10.1016/j.ndteint.2020.102309.
Nielsen, C.V., Zhang, W., Martins, P.A.F., Bay, N., 2015. 3D numerical simulation of projection welding of square nuts to sheets. J. Mater. Process. Technol. 215, 171–180. https://doi.org/10.1016/j.jmatprotec.2014.08.017.
Oswald-Tranta, B., 2016. Comparison of time and frequency behavior in TSR and PPT evaluation. In: Thermosense: Thermal Infrared Applications XXXVIII, 9861. SPIE, p. 98610P. https://doi.org/10.1117/12.2228864.
Oswald-Tranta, B., 2017. Time and frequency behaviour in TSR and PPT evaluation for flash thermography. Quant. InfraRed Thermogr. J. 14, 164–184. https://doi.org/10.1080/17686733.2017.1283743.
Palumbo, D., Cavallo, P., Galietti, U., 2019a. An investigation of the stepped thermography technique for defects evaluation in GFRP materials. NDT E Int. 102, 254–263. https://doi.org/10.1016/j.ndteint.2018.12.011.
Palumbo, D., D'Accardi, E., Galietti, U., 2019b. A new thermographic procedure for the non-destructive evaluation of RSW joints. SPIE Int. Soc. Opt. Eng. 23. https://doi.org/10.1117/12.2518979.
Parker, W.J., Jenkins, R.J., Butler, C.P., Abbott, G.L., 1961. Flash method of determining thermal diffusivity, heat capacity, and thermal conductivity. J. Appl. Phys. 32, 1679–1684. https://doi.org/10.1063/1.1728417.
Plonka, G., Potts, D., Steidl, G., Tasche, M., 2018. Fast Fourier transforms. Appl. Numer. Harmon. Anal. https://doi.org/10.1007/978-3-030-04306-3_5.
Pouranvari, M., Marashi, S.P.H., 2013. Critical review of automotive steels spot welding: process, structure and properties. Sci. Technol. Weld. Join. 18, 361–403. https://doi.org/10.1179/1362171813Y.0000000120.
Provencal, E., Laperrière, L., 2022. WeldNet: from 3D phased-array ultrasound scans to 3D geometrical models of welds and defects. CIRP Ann. 71, 445–448. https://doi.org/10.1016/j.cirp.2022.04.033.
Salazar, A., Mendioroz, A., Apiñaniz, E., Pradere, C., Noël, F., Batsale, J.C., 2014. Extending the flash method to measure the thermal diffusivity of semitransparent solids. Meas. Sci. Technol. 25 https://doi.org/10.1088/0957-0233/25/3/035604.
Santoro, L., Sesana, R., Molica Nardo, R., Curá, F., 2023. Infrared in-line monitoring of flaws in steel welded joints: a preliminary approach with SMAW and GMAW processes. Int. J. Adv. Manuf. Technol. 128, 2655–2670. https://doi.org/10.1007/s00170-023-12044-2.
Schlichting, J., Brauser, S., Pepke, L.A., Maierhofer, C., Rethmeier, M., Kreutzbruck, M., 2012. Thermographic testing of spot welds. NDT E Int. 48, 23–29. https://doi.org/10.1016/j.ndteint.2012.02.003.
Schramkó, M., Nyikes, Z., Tóth, L., Kovács, T.A., 2022. Investigation of the ultrasonic welded stainless steel corrosion resistance. J. Phys. Conf. Ser. 2315 https://doi.org/10.1088/1742-6596/2315/1/012028.
Schwenk E.B., Shearer G.D. Measuring projection weld strength by acoustic emission. 2023.
Sesana, R., Santoro, L., Curà, F., Molica Nardo, R., Pagano, P., 2023. Assessing thermal properties of multipass weld beads using active thermography: microstructural variations and anisotropy analysis. Int. J. Adv. Manuf. Technol. 128, 2525–2536. https://doi.org/10.1007/s00170-023-11951-8.
Shepard, S.M., Lhota, J.R., Ahmed, T., 2009. Measurement limits in flash thermography. In: Thermosense XXXI, 7299. SPIE, p. 72990T. https://doi.org/10.1117/12.820062.
Summerville, C., Adams, D., Compston, P., Doolan, M., 2017. Nugget diameter in resistance spot welding: a comparison between a dynamic resistance based approach and ultrasound C-scan. Procedia Eng. 183, 257–263. https://doi.org/10.1016/j.proeng.2017.04.033.
Summerville, C., Compston, P., Doolan, M., 2019. A comparison of resistance spot weld quality assessment techniques. Procedia Manuf. 29, 305–312. https://doi.org/10.1016/j.promfg.2019.02.142.
Thornton, M., Han, L., Shergold, M., 2012. Progress in NDT of resistance spot welding of aluminium using ultrasonic C-scan. NDT E Int. 48, 30–38. https://doi.org/10.1016/j.ndteint.2012.02.005.
Vavilov V. Evaluating the efficiency of data processing algorithms in transient thermal NDT. Thermosense XXVI, vol. 5405, 2004. 10.1117/12.537604.
Vavilov, V.P., Almond, D.P., Busse, G., Grinzato, E., Krapez, J.C., Maldague, X., Marinetti, S., Peng, W., Shirayev, V., Wu, D., 1998. Infrared thermographic detection and characterisation of impact damage in carbon fibre composites: results of the round robin test. Proceedings of the Quantitative Infrared Thermography (QIRT 98) 43–52.
Vavilov, V.P., Burleigh, D.D., 2015. Review of pulsed thermal NDT: physical principles, theory and data processing. NDT E Int. 73, 28–52. https://doi.org/10.1016/j.ndteint.2015.03.003.
Vavilov, V.P., Pawar, S.S., 2015. A novel approach for one-sided thermal nondestructive testing of composites by using infrared thermography. Polym. Test. 44, 224–233. https://doi.org/10.1016/j.polymertesting.2015.04.013.
Verspeek, S., Ribbens, B., Maldague, X., Steenackers, G., 2022. Spot weld inspections using active thermography. Appl. Sci. 12 https://doi.org/10.3390/app12115668 (Switzerland).
Vértesy, G., Tomáš, I., 2018. Nondestructive magnetic inspection of spot welding. NDT E Int. 98, 95–100. https://doi.org/10.1016/j.ndteint.2018.05.001.
Walther, D., Schmidt, L., Schricker, K., Junger, C., Bergmann, J.P., Notni, G., et al., 2022. Automatic detection and prediction of discontinuities in laser beam butt welding utilizing deep learning. J. Adv. Join. Process. 6 https://doi.org/10.1016/j.jajp.2022.100119.
Wang, X., Zhang, Y., 2017. Effects of welding procedures on resistance projection welding of nuts to sheets. ISIJ Int. 57, 2194–2200. https://doi.org/10.2355/isijinternational.ISIJINT-2017-219.
Waugh, R.C., Dulieu-Barton, J.M., Quinn, S., 2014. Modelling and evaluation of pulsed and pulse phase thermography through application of composite and metallic case studies. NDT E Int. 66, 52–66. https://doi.org/10.1016/j.ndteint.2014.04.002.

Xia, Y.J., Su, Z.W., Li, Y.B., Zhou, L., Shen, Y., 2019. Online quantitative evaluation of expulsion in resistance spot welding. J. Manuf. Process. 46, 34–43. https://doi.org/10.1016/j.jmapro.2019.08.004.

Yetilmezsoy, K., Erhuy, C.G., Ates, F., Bilgin, M.B., 2018. Implementation of fuzzy logic approach to estimate the degree of expulsion and spattering index and weld strength in projection welding. J. Braz. Soc. Mech. Sci. Eng. 40 https://doi.org/10.1007/s40430-018-1210-9.

Zhao, D., Ren, D., Song, G., Zhao, K., Liu, L., Zhang, Z., 2020. Comparison of mechanical properties and the nugget formation of composite ceramic-centered annular welding and traditional resistance spot welding. Int. J. Mech. Sci. 187 https://doi.org/10.1016/j.ijmecsci.2020.105933.